Deconstructing cell size control into physiological modules in *Escherichia coli*

Authors:
Fangwei Si[1]†, Dongyang Li[2]†, Sarah E. Cox[1]†, John T. Sauls[1], Omid Azizi[3], Amy B. Schwartz[1], Michael J. Erickstad[1], Yonggun Jun[1], Xintian Li[1], Suckjoon Jun[1,2]*

Affiliations:
[1] Department of Physics, University of California San Diego, 9500 Gilman Dr, La Jolla, CA 92093
[2] Section of Molecular Biology, Division of Biology, University of California San Diego, 9500 Gilman Dr, La Jolla, CA 92093
[3] Department of Bioengineering, University of California San Diego, 9500 Gilman Dr, La Jolla, CA 92093

* Correspondence to: Suckjoon Jun (suckjoon.jun@gmail.com).
†These authors contributed equally to this work.

Cell size homeostasis is a basic aspect of coordinated biosynthesis during steady-state growth, yet it was unknown how physiological control and the cell cycle are linked. We show that the cellular resources required to start growth and one round of replication is constant. This "unit cell" size remains invariant under extensive perturbations to replication rate, transcription, translation, ribosome content, lipid and cell wall synthesis, surface-to-volume ratio of the cell, cell shape, and cell division. Instead, the unit cell is exclusively determined by the process of replication initiation. We demonstrate that cell size control in *Escherichia coli* is completely characterized by three functionally distinct modules – the unit cell, growth and the cell cycle. This leads to the general growth law that cell size is the sum of all unit cells. The general growth law explains how growth and the cell cycle are coordinated and quantitatively predicts cell size for any steady-state growth condition.

For faithful reproduction, a cell must coordinate synthesis of DNA, protein, and cell envelope. Cell size homeostasis is one of the fundamental consequences of that coordination, with the ultimate outcomes of all intracellular processes being the growth rate, cell shape, and cell size. We have studied this coordinated synthesis to understand the basic principle of cell size control in the model organism *E. coli*.

Two quantitative, phenomenological observations established the foundation of bacterial physiology. The first experimental observation is that the average cell size, $S(\lambda)$, has an exponential dependence on the nutrient-imposed growth rate λ. This result is summarized as the "growth law"

$$S(\lambda) = S_0 \exp(\gamma \cdot \lambda), \qquad (1)$$

where S_0 and γ are constants, and the growth rate is related to the generation time τ as $\lambda=\ln 2/\tau$ (see below) (Fig. 1b) (*1*). The second experimental observation is that the duration of chromosome replication is constant for a wide range of growth rates (Fig. 1e), which became the basis of the bacterial cell cycle model (*2, 3*). If both of these observations are valid, the slope constant γ should be related to the duration of the cell cycle such that the average number of overlapping cell cycles is given by $\exp(\gamma\cdot\lambda)$ (*4*). Consequently, the constant $S_0 = S(\lambda)/\exp(\gamma\cdot\lambda)$ would be the cell size per one round of cell cycle regardless of the nutrient conditions (*4*).

There are several important issues. First, the constancy of S_0 is often interpreted as active coordination between growth and the replication cycle in *E. coli*, whereby replication initiates when the cell reaches a threshold size. However, this has been a subject of active debate due to a lack of conclusive data (*4–11*). Recent study has even proposed that size control is in fact imposed at cell division, not at replication initiation (*10*). Second, size vs. growth rate of individual cells systematically deviates from the growth law, raising a question whether the growth rate actually determines the cell size (*12, 13*). Third, the growth law only specifies the size (volume) of the cell based on the growth rate, whereas recent work has proposed that a surface-to-volume ratio is a key determinant of cell size (*14*).

Another major related question is how cells allocate cellular resources to intracellular processes (*15*). This has important implications for size control, because proteins constitute most of the cellular dry mass (*16*). Recent studies have suggested that the total proteome in a steady-state population is partitioned, and optimal growth requires the ribosomal fraction of the proteome to increase linearly with the growth rate (Fig. 1d) (*17*). However, proteome partitioning cannot determine total proteins per cell. Furthermore, cell cycle proteins are a small fraction of the total proteins (*15, 18, 19*). Therefore, population-level approaches focusing on the average proteome composition have intrinsic limitations in understanding cell size control.

In this study, we present a concept of the "unit cell" - the basic building block of cell size. The unit cell represents the invariant minimal cellular resources required to start growth and one round of replication cycle for any growth condition. We show that cells coordinate their growth and cell cycle such that cell size is the sum of all unit cells, wherein the total number of unit cells is determined by the number of all ongoing replication cycles. This provides a mechanistic overarching principle of cell size control and coordination principle with quantitative predictive power.

Multiplexing physiological measurements

Our goal was to understand the relationship between physiological control and cell size. In particular, we wanted to measure how cellular resources are allocated to functionally distinct intracellular processes during steady-state growth. This requires simultaneous measurements of several growth parameters over a wide range of growth conditions and physiological perturbations. To this end, we developed a multiplex turbidostat and a high-throughput analysis system (Fig. 1a; see Supplementary Information).

Experimental results for normal growth conditions (namely, cell culture without any inhibition) are summarized in Fig. 1. The average size of the cells showed an exponential dependence on the nutrient-imposed growth rate, reproducing the growth law (Fig. 1b) (*1, 12*). The cell shape measured by aspect ratio of the cell was constant for all growth conditions (Fig. 1c). Since cell volume increases without changing cell shape, this leads to systematic decrease in the surface-to-volume ratio as the growth rate increases (Fig. 1c).

The ribosome fraction, measured using the same samples, exhibited a linear relationship with the growth rate (Fig. 1d) as shown previously (*16, 20*). The simultaneous change in protein composition and exponential increase in cell size are illustrated in Fig. 1b (right).

We also measured the duration of chromosome replication (C period) and the time elapsed between termination of replication and cell division (D period) (Fig. 1e and Extended Data Fig. 2b). C period and the duration of the cell cycle (C+D period) were constant (C = 38.0 ± 4.5 minutes and C+D = 75.1 ± 7.2 minutes), in quantitative agreement with known results (Fig. 1e and Extended Data Fig. 2a) (*3, 5, 16, 21*).

These results demonstrate that our multiplex system ensures steady-state growth and simultaneous measurements of physiological parameters such as cell size, cell cycle, and ribosome content.

Decoupling replication from growth

A major hypothesis in bacterial physiology is that DNA replication can be decoupled from growth, and the cell size should change accordingly (*22*). Testing this prediction requires experimental means to change the duration of DNA replication independent of the growth physiology. Following previous suggestions (*23*), we constructed a *thyA*- strain that requires thymine supplementation for viability. Since thymine enters the cell by passive diffusion, the intracellular level of thymine can be modulated by adjusting the concentration of thymine supplied in the growth media. When thymine concentration is below saturation, known as thymine limitation, the nucleotide pools in the cell become reduced, leading to an increase in the replication period (*24, 25*).

When thymine concentration drops below a certain threshold, the growth of *thyA*- eventually halted, in line with previous observations of "thymineless death" (*25–27*). At intermediate thymine concentrations, the *thyA*- strain maintained steady-state growth under thymine limitation with a constant growth rate similar to wildtype (Fig. 2a). The C period however increased nearly twofold, from approximately C = 41 minutes to nearly C = 70 minutes (Fig. 2b), showing clear decoupling from growth. The ribosomal fraction of the proteome remained unchanged (Extended Data Fig. 2e), consistent with the view that the growth rate is solely determined by the fraction of active ribosomes (*17, 20*).

The prolonged replication period had non-trivial consequences on the cell cycle (Fig. 2d). During thymine limitation, C+D increased from approximately one hour up to three hours, whereas the

generation time stayed constant ($\tau \approx 1$ hour) (Fig. 2c). Since the number of overlapping cell cycles is given by the ratio (C+D)/τ, up to three cell cycles were forced to overlap. To validate this independently, we directly visualized the replication origin region using ParB-mCherry with a *parS* site inserted at 84.3' near *ori* (*28*). Indeed, we observed that both the cell size and the number of ParB-mCherry foci simultaneously increased in our experiments despite potential cohesion of replicated chromosomal loci (Fig. 2d) (*29*).

Intriguingly, the morphology of the cell changed from a rod shape to a less well-defined round shape with a larger diameter during thymine limitation (Fig. 2c and Extended Data Fig. 2c) (*30, 31*). Thus, the increase in C+D can be attributed to the change in both replication period and the morphology, since it should take longer for the synthesis and assembly of the division machinery along the increased circumference of the cell.

Our results provide direct evidence for the predicted relationship between cell size and the cell cycle period. If C period increases to C+ΔC without affecting the growth rate λ, the cell size should increase exponentially by a factor of $\exp[\Delta C \cdot \lambda]$ according to the growth law [equation (1)]. This is the case for thymine limitation, and our results indeed show an increase in size by a factor of $\exp[\Delta(C+D) \cdot \lambda]$ for an increase in C+D by Δ(C+D) (Fig. 2c and Extended Data Fig. 2d). Furthermore, $S_0 = S(\lambda)/\exp[(C+D) \cdot \lambda]$ was constant for both normal growth and thymine limitation (Fig. 2c).

Constancy of the unit cell under translational inhibition

If cell size and growth rate are positively correlated as in the growth law, inhibition of protein synthesis should result in simultaneous decrease in both. However, our data showed complex changes in cell size over different media and levels of translational inhibition (Fig. 3a). We measured cell size under translational inhibition using sublethal concentrations of chloramphenicol, which irreversibly binds to one of the subunits of the ribosome and blocks protein synthesis. In fast-growth conditions, the cell size initially decreased, and then increased with increasing growth inhibition. In contrast, in slow-growth conditions, the cell size increased despite decrease in growth rate. In intermediate growth conditions, cell size remained unchanged (*32*). In other words, cell size changed in an unpredictable way with regards to growth rate.

Puzzled by this unexpected patterns in cell size, we tested if the changes in cell size were caused by changes in the replication period during translational inhibition, as in the case of thymine limitation. However, C period always increased by chloramphenicol treatment regardless of the growth conditions (*33*), and there appeared to be no obvious relationship with the cell size (Fig. 3a, b and Extended Data Fig. 4, 5f).

Since total proteins *per cell* is a good proxy for cell size, we asked if the differential changes in cell size (Fig. 3a) can be attributed to an underlying control by protein composition (Fig. 3d). For example, in the fastest growth conditions, translational inhibition causes a rapid decrease in growth rate but a slow

change in the fraction of non-ribosomal proteins, φ_x (Fig. 3d) (*20*). Thus, if the cell cycle solely depends on φ_x, the cell would divide at a smaller size because the cell grows more slowly while the cell division cycle proceeds normally. Similarly, in the slowest growth conditions, φ_x decreases rapidly while the growth rate remains constant. This would cause an increase in cell size due to delayed division. Models relying solely on protein composition were unable to determine the absolute size of the cell, because cell size can freely scale without changing protein composition, e.g., φ_x. We made various attempts to connect protein composition and cell size by introducing ad-hoc assumptions, all in vain.

To our surprise, we discovered that the average cell size per number of replication origins (size/*ori*), calculated by $S(\lambda)/\exp[(C+D)\cdot\lambda]$ [equation (1)], remained unchanged despite extensive growth inhibition (Fig. 3e). This was unexpected for several reasons. First of all, cell size no longer showed an exponential dependence on the growth rate during growth inhibition (Fig. 3a). Translational inhibition also significantly altered the replication kinetics in a growth condition dependent manner (Fig. 3b). Furthermore, protein composition was also altered significantly by growth inhibition (Fig. 3d). Since the basic assumptions underlying the notion of initiation mass did not hold during translational inhibition, there was no apparent reason that size/*ori* should still be constant.

We verified the constancy of size/*ori* for all 163 independent sets of chloramphenicol experiments (Fig. 3e). The distribution of size/*ori* was Gaussian, and its average coincided with S_0 of the growth law under normal growth conditions [equation (1)]. The constancy of size/*ori* under translational inhibition was reinforced by three additional observations. (1) The changes in the cell size and the number of replication origins resembled each other (Fig. 3a, c). (2) The number of fluorescent foci labeling the *ori* region was consistent with the number of replication origins measured by qPCR (Extended Data Fig. 3d, g). (3) Cell size per one chromosome equivalent genome content also did not change from normal growth conditions (Extended Data Fig. 2f).

A conceptual, basic "unit cell" of cellular resources emerges from these results (*34*). In the original growth law, the unit cell represents the limit of cellular resources as the growth rate approaches zero (Fig. 1b). The size of the unit cell is S_0, proportional to the initiation mass per *ori* (*4, 34, 35*). Therefore, each unit cell contains one genome equivalent DNA and the minimal cellular resources required for growth and to initiate the cell cycle.

Invariance of the unit cell under extensive physiological perturbations

While the constancy of size/*ori* has been well recognized for normal growth conditions [equation (1)] (*4, 11*), its constancy under translational inhibition has never been reported (Fig. 3; see previous section). To understand the extent to which the unit cell is invariant under growth inhibition, we expanded perturbation experiments using several other antibiotics that inhibit biomolecule synthesis.

First, we tested the effect of erythromycin. Chloramphenicol and erythromycin inhibit protein synthesis, although their modes of action are different. Indeed, changes in the ribosomal content by the two

antibiotics were virtually indistinguishable from each other (Extended Data Fig. 2h). However, erythromycin had qualitatively different effects on both cell size and the cell cycle. In slow and medium growth conditions (glycerol and glucose minimal media, respectively), cell size increased dramatically as growth rate gradually decreased, and the C+D period was prolonged even more steeply by erythromycin (Extended Data Fig. 2g, 5a–c). Despite these differences, the unit cell always remained invariant (Fig. 3e).

Second, we inhibited transcription using rifampicin, which binds to RNA polymerase and blocks RNA synthesis. As the concentration of rifampicin increased, the growth rate (Fig. 3e) and the ribosomal content decreased monotonically (Extended Data Fig. 5d). However, in stark contrast to translational inhibition, neither cell size nor the cell cycle were significantly affected (Extended Data Fig. 5d). Again, the unit cell remained constant (Fig. 3e).

Third, we inhibited the synthesis of fatty acids using triclosan. Fatty acids are a major constituent of the cell-wall membrane, and their synthesis has been shown to affect cell size (*36, 37*). Both cell size and C+D period increased with increasing triclosan concentration, but their patterns differed from those caused by translational or transcriptional inhibition (Extended Data Fig. 5e). In particular, at higher concentrations of triclosan, we observed frequent filamentation and delayed cell division (Extended Data Fig. 5e). Nevertheless, the unit cell remained invariant (Fig. 3e).

The invariance of the unit cell under extensive physiological perturbations suggests that the control of unit cell is robust to changes in its composition. In other words, the unit cell is an invariant basic building block of cellular resources, equivalent to a constant initiation mass (Fig. 3f), for any steady-state growth condition.

Replication initiation alone is linked to the unit cell

An obvious question is what determines the unit cell. Our results indicated that perturbations to biomolecule synthesis machinery or replication kinetics have no effect on the unit cell. One possibility is that the unit cell is coordinated with the timing of the cell cycle, independent of growth. For example, if *dnaC* temperature-sensitive mutants were grown at nonpermissive temperature with inhibition in cell division, size/*ori* would increase indefinitely and cells become inviable (*38, 39*). If replication initiation can somehow be delayed without affecting cell growth and division, the unit cell size should increase while the cells remain viable.

These ideas can be tested by knockdown experiments on several genes involved in replication initiation in *E. coli*. We developed a CRISPR-dCas9 based tunable suppression system, "tCRISPRi," to control gene expression. The tCRISPRi system allows precise and continuous titration of gene expression by more than 10-fold relative to the wild-type expression level using a plasmid-free system (unpublished data). We used tCRISPRi and repeated under- and over-initiation experiments (*40*) to measure the unit cell size and the protein composition under these conditions.

We examined DnaA, one of the most widely conserved initiator proteins (*41*). Its suppression causes under-initiation and increases the overall cell size (*40*), which should increase the cell size at initiation (*42*) and thus the unit cell size. We constructed a DnaA knockdown tCRISPRi strain with a fluorescent transcriptional reporter. When the expression level of *dnaA* decreased to approximately 30% of the wild type level, the unit cell monotonically increased by almost two-fold (Fig. 4a). Consistent with the increase in unit cell size due to under-initiation, the genome content per cell decreased as expected (Fig. 4b).

We also tested SeqA, a major negative modulator of replication initiation in *E. coli*, whose suppression induces over-initiation of DNA replication (*43, 44*). We found that the unit cell gradually decreased during SeqA knockdown by tCRISPRi (Fig. 4a), and the genome content per cell increased (Fig. 4b). SeqA knockdown did not affect physiology otherwise, and the growth rate and ribosome content remained at the wild type values (Extended Data Fig. 6b). Instead, SeqA knockdown selectively decreased the unit cell size (Fig. 4a).

The unit cell is independent of cell shape and division

Since replication initiation is linked to the unit cell, we wondered whether cell division as a major cell cycle event also affects the unit cell. Previously, the cell diameter and C+D period increased simultaneously during thymine limitation (Fig. 2). We therefore set out to perturb cell shape to study its impact on cell division and the unit cell.

An actin homolog MreB was a promising candidate because of its role in cell shape maintenance in *E. coli* (*45, 46*). Since *mreB* is an essential gene, we used our tCRISPRi system and systematically knocked down *mreB*. Cells gradually transitioned from rod to round shape during *mreB* knockdown, consistent with recent results based on CRISPR interference in *B. subtilis* (Fig. 5a) (*47*), while both cell size and C+D period increased (Fig. 5a). In contrast to these changes, C period, growth rate, and ribosome content all stayed at their wild type values and the unit cell remained invariant. These results suggest that the increase in C+D was exclusively caused by a delay in cell division, leading to the increase in cell size (Fig. 5a).

We also inhibited cell wall synthesis using fosfomycin, which inactivates MurA, an enzyme required for peptidoglycan biosynthesis. Fosfomycin treated cells maintained a rod shape, but their surface-to-volume ratio decreased (Fig. 5b), in agreement with recent work (*14*). Nevertheless, the unit cell remained invariant (Fig 5b).

We conclude that cell shape affects the kinetics of cell division, which in turn can change C+D and therefore cell size, independently from growth and DNA replication. Above all, the unit cell is invariant under perturbations to cell shape, surface-to-volume ratio, or cell division.

Discussion

In the present work, we performed a series of experiments to decouple growth and the cell cycle to understand how physiological controls are linked to cell size. Three functionally distinct physiological modules emerged (*48*). The center of this modular architecture of physiology is the invariant unit cell, which is equivalent to the cellular resources required to start and maintain one round of cell cycle. The unit cell is the limit as the growth rate approaches zero in the growth law (Fig. 1b). Therefore, each unit cell contains one genome equivalent of DNA and the minimal cellular resources required to start growth and the cell cycle. The invariance of the unit cell is largely independent of molecular details and robust to physiological (e.g., biomolecule synthesis) and cell biological (e.g., cell shape) perturbations.

Our experimental results for cell size control can be summarized as the general growth law with predictive power for any steady-state growth [equation (2); Fig. 6]:

$$\underbrace{S}_{\text{cell size}} = \underbrace{S_0}_{\text{unit cell}} \times \underbrace{2^{\overbrace{(\mathrm{C+D})/\tau}^{\text{num. overlapping cell cycles}}}}_{\text{num. unit cells}} = S_0 \times e^{\overbrace{(\mathrm{C+D})}^{\text{cell cycle}}\overbrace{\lambda}^{\text{growth}}} \qquad (2)$$

The unit cell is the basic building block of cellular resources of the cell, and cell size is the sum of all unit cells controlled by replication initiation [Fig. 3f; equation (2)]. The general growth law consists of, and coordinates, three functionally distinct physiological modules representing the unit cell (S_0), growth (λ), and the cell cycle (C+D). These three modules can be decoupled by physiologically or genetically perturbing each module selectively (Figs. 2–5). For special cases of S_0 and C+D are both constant independent of growth conditions, the general growth law reduces to the original growth law.

Considering the invariance of the unit cell under extensive physiological perturbations, and the universal nature of the biological modules in equation (2), the modular architecture of the general growth law may represent an overarching quantitative framework for cell size control in single-cell organisms.

Figures

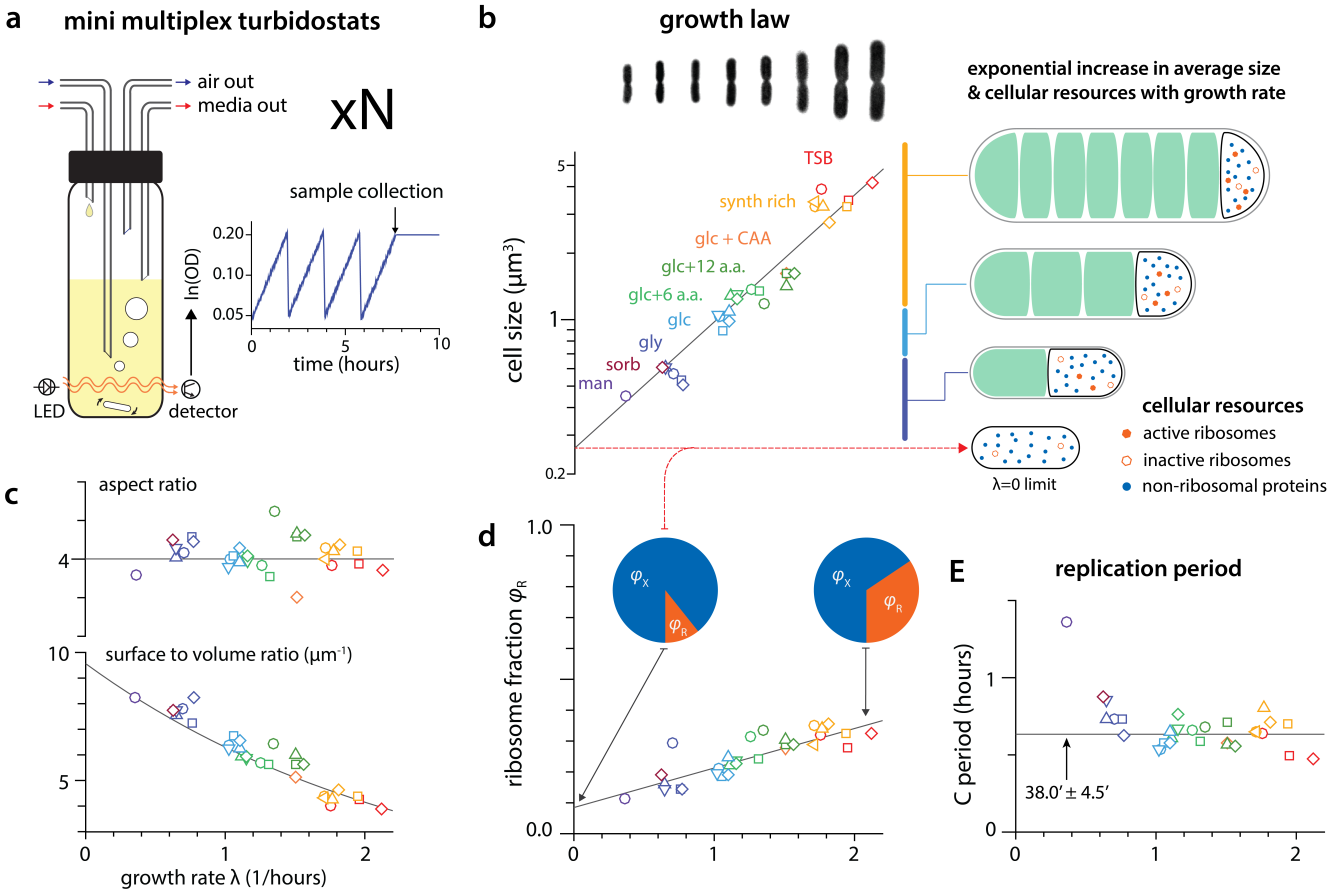

Figure 1 Multiplexing physiological measurements.

a, Computer-controlled multiplex mini turbidostats. All data in (**b**-**e**) are from the same samples. **b**, Growth law for normal growth conditions of an *E. coli* K12 NCM3722 strain. Each data point represents order of 10^4 cells (see detailed sample size in Supplementary Table 1). Solid line is an exponential fit to data. In the illustration on the right, cell size at replication initiation is integer multiples of the cell size at λ =0 limit. In each unit volume, the number of (active) ribosomes increases linearly as the growth rate increases. **c**, Top: aspect ratio of the cells remains constant in all normal growth conditions. Bottom: surface-to-volume ratio of the cells decreases as the growth rate increases. Solid line was calculated assuming the cell is rod-shaped with the measured aspect ratio and cell volume. **d**, Linear relationship between the average ribosome fraction and the growth rate. **e**, Replication period (C period) is constant for growth rate $\lambda > 0.8$ (or generation time $\tau = \ln 2/\lambda < 52$ minutes). Solid line indicates average C period for $\lambda > 0.8$.

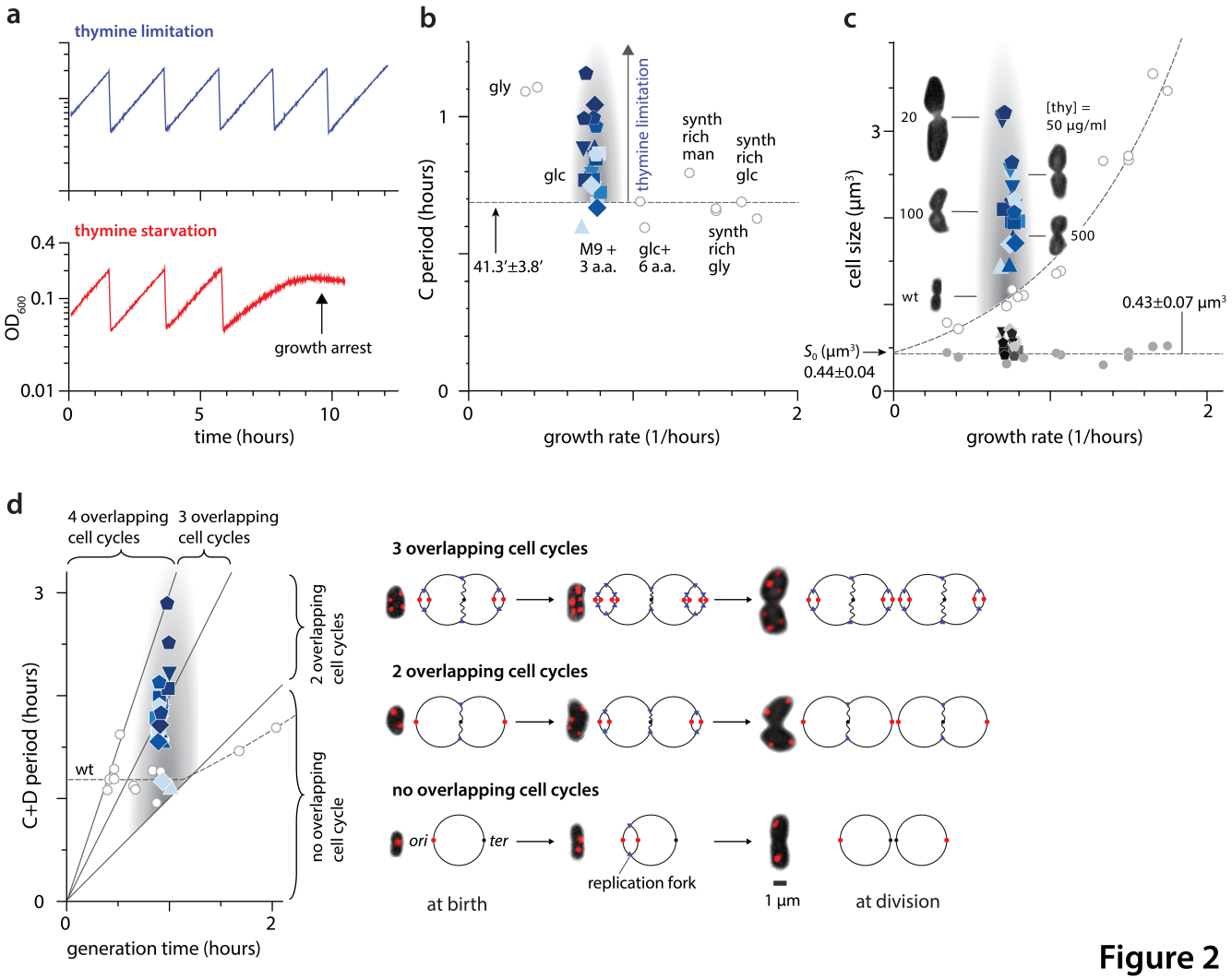

Figure 2

Figure 2 Decoupling replication from growth by thymine limitation

a, Typical growth curves of an MG1655 *thyA*- strain from mini turbidostats. Cells exhibit steady-state growth under thymine limitations, whereas they show growth arrest under thymine starvation[25]. Only steady-state growth samples were collected and analyzed in the present study. **b**, Systematic increase of C period at constant growth rate under thymine limitation. Dashed line is the average C period of normal growth of MG1655 (*thyA*+) cells for $\lambda > 0.7$. **c**, Cells increase in size under thymine limitation, developing into irregular shape. Cell size per *ori* agrees with the predicted S_0 of the growth law [equation (1)] for both *thyA*- and *thyA*+ strains. **d**, Left: The number of overlapping cell cycles increases from 2 to 3 under thymine limitation due to increase in the cell cycle period (C+D), while the growth rate remains unchanged. The dashed line indicates the change of overlapping cell cycle number for normal growth conditions. Right: Cytological confirmation of increasing overlapping cell cycles. The *ori* region was directly visualized using ParB-mCherry with *parS* sequence inserted near *ori* at 84.3'.

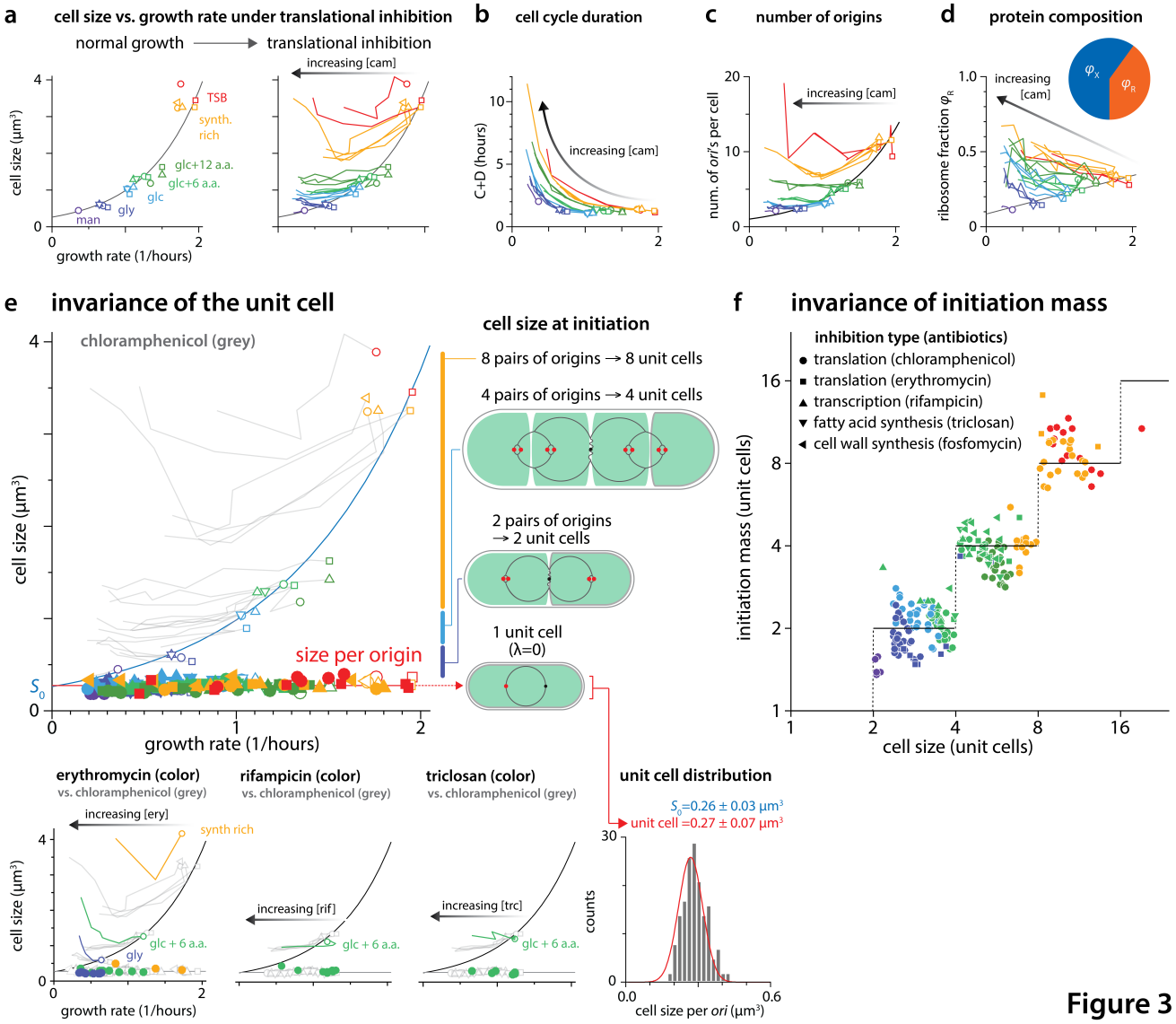

Figure 3

Figure 3 Invariance of the unit cell under extensive physiological perturbations.

a, Left: Cell size increases exponentially as a function of nutrient-imposed growth rate for normal growth conditions. Right: Cell size changes non-monotonically and nonlinearly in response to translational inhibition by chloramphenicol. **b**, C+D always increases in chloramphenicol-treated cells. **c**, Number of replication origins changes in a similar manner as changes in cell size in (**a**). Solid line is a fit for normal growth data using the cell cycle model[4]. **d**, Ribosomal fraction ϕ_R of the total proteins increases linearly under chloramphenicol treatment. **e**, Top left: size/*ori* remains constant despite translational inhibition by chloramphenicol, and agrees with S_0 of the original growth law. Top right: illustrations showing that cell size is sum of all "unit cells", where the size of the unit cell is obtained in the size limit $\lambda \to 0$ in the growth law. Bottom left: the unit cell remains invariant under translational inhibition by erythromycin, transcriptional inhibition by rifampicin, and lipid synthesis inhibition by triclosan. Bottom right: The distribution of the unit cell size is Gaussian, and its mean coincides with S_0. In this Figure, each data line represents an order of 10^4 data points. **f**, Invariance of initiation mass under inhibition of biomolecule synthesis (see the calculation in Supplementary Information). Symbols are the data. Solid lines are the prediction from the general growth law [equation (2)]. Different colors reflect different growth media used in the experiments, consistent with the coloring scheme in Fig. 1b and 3a.

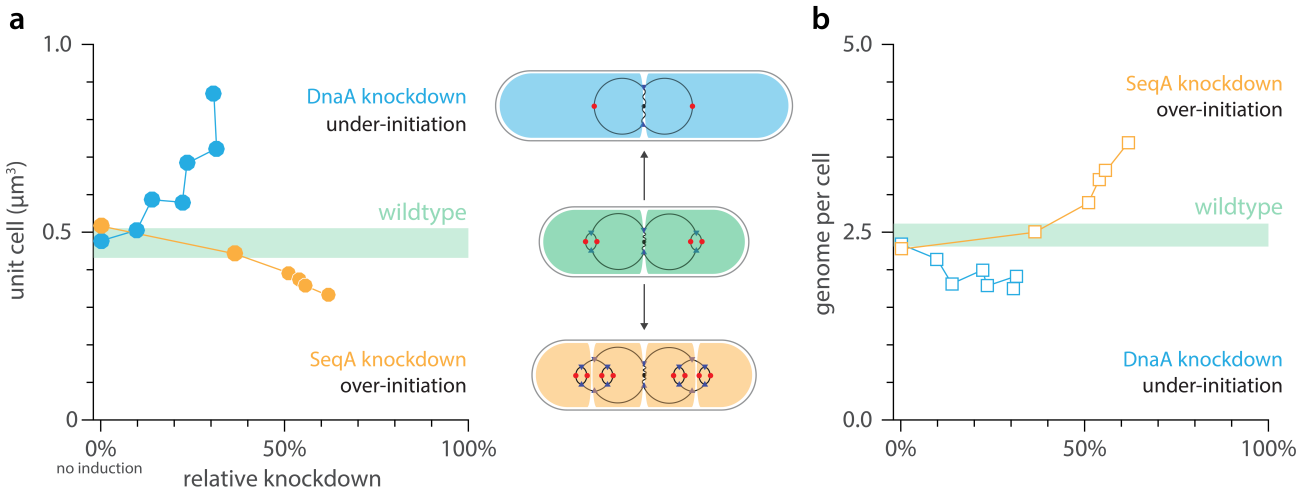

Figure 4

Figure 4 Replication initiation alone is linked to the unit cell.

a, Left: The unit cell size increases as the expression level of initiator gene *dnaA* is systematically suppressed by tCRISPRi. In contrast, the unit cell size decreases when a negative modulator gene *seqA* is knocked down. The horizontal band indicates the average unit cell size without gene expression knockdown. The width of the band indicates +/- one standard deviation. Right: Illustration of the impact of under-initiation (DnaA knockdown) and over-initiation (SeqA knockdown) on the unit cell. **b**, Per-cell genome content decreases with under-initiation, and increases with over-initiation, consistent with (**a**).

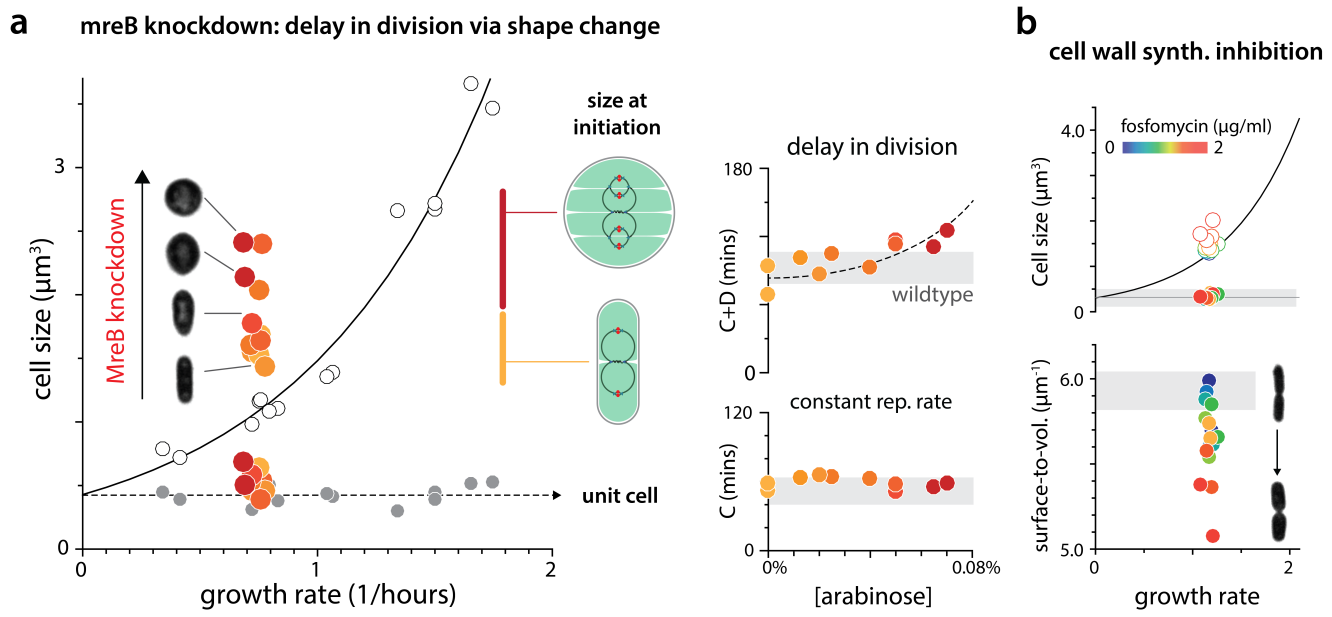

Figure 5

Figure 5 The unit cell is independent of cell shape, surface-to-volume ratio, and cell division. **a**, Left: Knockdown of MreB causes cell shape changes from rod to round, but does not change the growth rate or the replication rate (bottom-right). Instead, change in cell shape by MreB knockdown causes delay in cell division (top-right), and therefore the cell size. **b**, Inhibition of cell-wall synthesis causes decrease in surface-to-volume ratio. In both (**a**) and (**b**), the unit cell remains invariant. The grey horizontal lines in (**a**) and (**b**) indicate the average value of the wildtype strain with thickness of the line representing +/- one standard deviation.

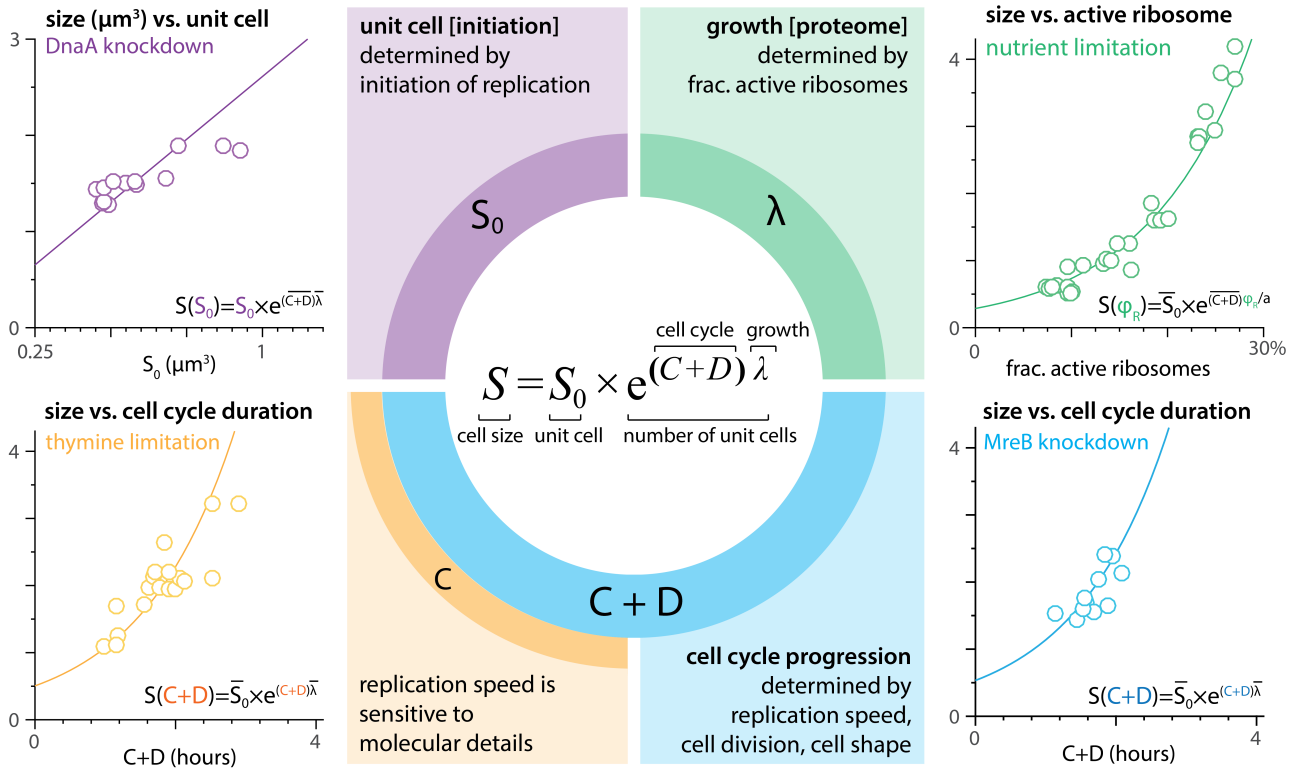

Figure 6

Figure 6 The general growth law with quantitative predictive power.

The general growth law deconstructs the cell size control into three biologically universal, distinct physiological modules. (clockwise from top-left) The unit cell size (S_0) is exclusively linked to replication initiation; growth rate λ is determined by the active fraction of the ribosomes of the total cellular resources; C+D controls division timing. These physiological modules can be decoupled by physiologically or genetically perturbing each module individually. Even when the perturbation changes multiple modules simultaneously, the modules are coordinated such that cell size is the sum of all unit cells. The quantitative predictive power of the general growth law is demonstrated as the solid lines against the data in the four quadrants, which are not subject to any adjustable parameters.

References

1. Schaechter, M., Maaløe, O. & Kjeldgaard, N. O. Dependency on Medium and Temperature of Cell Size and Chemical Composition during Balanced Growth of *Salmonella typhimurium*. *Microbiology* **19,** 592–606 (1958).
2. Cooper, S. & Helmstetter, C. E. Chromosome replication and the division cycle of *Escherichia coli* B/r. *J. Mol. Biol.* **31,** 519–540 (1968).
3. Helmstetter, C. E. & Cooper, S. DNA synthesis during the division cycle of rapidly growing *Escherichia coli* B/r. *J. Mol. Biol.* **31,** 507–518 (1968).
4. Donachie, W. D. Relationship between cell size and time of initiation of DNA replication. *Nature* **219,** 1077–1079 (1968).
5. Skarstad, K., Steen, H. B. & Boye, E. Cell cycle parameters of slowly growing *Escherichia coli* B/r studied by flow cytometry. *J. Bacteriol.* **154,** 656–662 (1983).
6. Bates, D. & Kleckner, N. Chromosome and replisome dynamics in *E. coli*: loss of sister cohesion triggers global chromosome movement and mediates chromosome segregation. *Cell* **121,** 899–911 (2005).
7. Cooper, S. Regulation of DNA synthesis in bacteria: analysis of the Bates/Kleckner licensing/initiation-mass model for cell cycle control. *Mol. Microbiol.* **62,** 303–307 (2006).
8. Wang, X., Lesterlin, C., Reyes-Lamothe, R., Ball, G. & Sherratt, D. J. Replication and segregation of an *Escherichia coli* chromosome with two replication origins. *Proc. Natl. Acad. Sci. U.S.A.* **108,** E243–250 (2011).
9. Hill, N. S., Kadoya, R., Chattoraj, D. K. & Levin, P. A. Cell size and the initiation of DNA replication in bacteria. *PLoS Genet.* **8,** e1002549 (2012).
10. Taheri-Araghi, S. Self-consistent examination of Donachie's constant initiation size at the single-cell level. *Front. Microbiol.* **6,** 208102 (2015).
11. Campos, M. *et al.* A Constant Size Extension Drives Bacterial Cell Size Homeostasis. *Cell* **159,** 1433–1446 (2014).
12. Taheri-Araghi, S. *et al.* Cell-Size Control and Homeostasis in Bacteria. *Curr. Biol.* **25,** 1–7 (2015).
13. Kennard, A. S. *et al.* Individuality and universality in the growth-division laws of single *E. coli* cells. *Phys. Rev. E* **93,** 012408 (2016).
14. Harris, L. K. & Theriot, J. A. Relative Rates of Surface and Volume Synthesis Set Bacterial Cell Size. *Cell* **165,** 1479–1492 (2016).
15. Li, G.-W., Burkhardt, D., Gross, C. & Weissman, J. S. Quantifying absolute protein synthesis rates reveals principles underlying allocation of cellular resources. *Cell* **157,** 624–635 (2014).
16. Bremer, H. & Dennis, P. P. Modulation of Chemical Composition and Other Parameters of the Cell at Different Exponential Growth Rates. *EcoSal. Plus* **3,** (2008).
17. Scott, M., Klumpp, S., Mateescu, E. M. & Hwa, T. Emergence of robust growth laws from optimal regulation of ribosome synthesis. *Mol. Syst. Biol.* **10,** 747 (2014).
18. Hui, S. *et al.* Quantitative proteomic analysis reveals a simple strategy of global resource allocation in bacteria. *Mol. Syst. Biol.* **11,** 784 (2015).
19. Schmidt, A. *et al.* The quantitative and condition-dependent *Escherichia coli* proteome. *Nat. Biotechnol.* **34,** 104–110 (2016).
20. Scott, M., Gunderson, C. W., Mateescu, E. M., Zhang, Z. & Hwa, T. Interdependence of cell growth and gene expression: origins and consequences. *Science* **330,** 1099–1102 (2010).
21. Stokke, C., Flåtten, I. & Skarstad, K. An easy-to-use simulation program demonstrates variations in bacterial cell cycle parameters depending on medium and temperature. *PLoS ONE* **7,** e30981 (2012).
22. Zaritsky, A. & Pritchard, R. H. Changes in Cell Size and Shape Associated with Changes in the

Replication Time of the Chromosome of *Escherichia coli*. *J. Bacteriol.* **114,** 824–837 (1973).
23. Pritchard, R. H. & Zaritsky, A. Effect of thymine concentration on the replication velocity of DNA in a thymineless mutant of *Escherichia coli*. *Nature* **226,** 126–131 (1970).
24. Zaritsky, A., Woldringh, C. L., Einav, M. & Alexeeva, S. Use of thymine limitation and thymine starvation to study bacterial physiology and cytology. *J. Bacteriol.* **188,** 1667–1679 (2006).
25. Khodursky, A., Guzmán, E. C. & Hanawalt, P. C. Thymineless Death Lives On: New Insights into a Classic Phenomenon. *Microbiology* **69,** 247–263 (2015).
26. Ahmad, S. I., Kirk, S. H. & Eisenstark, A. Thymine metabolism and thymineless death in prokaryotes and eukaryotes. *Annu. Rev. Microbiol.* **52,** 591–625 (1998).
27. Itsko, M. & Schaaper, R. M. dGTP Starvation in *Escherichia coli* Provides New Insights into the Thymineless-Death Phenomenon. *PLoS Genet.* **10,** e1004310 (2014).
28. Nielsen, H. J., Ottesen, J. R., Youngren, B., Austin, S. J. & Hansen, F. G. The *Escherichia coli* chromosome is organized with the left and right chromosome arms in separate cell halves. *Mol. Microbiol.* **62,** 331–338 (2006).
29. Sunako, Y., Onogi, T. & Hiraga, S. Sister chromosome cohesion of *Escherichia coli*. *Mol. Microbiol.* **42,** 1233–1241 (2001).
30. Meacock, P. A., Pritchard, R. H. & Roberts, E. M. Effect of Thymine Concentration on Cell-Shape in Thy$^-$ *Escherichia coli* B/r. *J. Bacteriol.* **133,** 320–328 (1978).
31. Zaritsky, A. & Woldringh, C. L. Chromosome replication rate and cell shape in *Escherichia coli*: lack of coupling. *J. Bacteriol.* **135,** 581–587 (1978).
32. Basan, M. *et al.* Inflating bacterial cells by increased protein synthesis. *Mol. Syst. Biol.* **11,** 836–836 (2015).
33. Pato, M. L. Alterations of the rate of movement of deoxyribonucleic acid replication forks. *J. Bacteriol.* **123,** 272–277 (1975).
34. Donachie, W. D. & Begg, K. J. Growth of the bacterial cell. *Nature* **227,** 1220–1224 (1970).
35. Donachie, W. D. & Blakely, G. W. Coupling the initiation of chromosome replication to cell size in *Escherichia coli*. *Curr. Opin. Microbiol.* **6,** 146–150 (2003).
36. Yao, Z., Davis, R. M., Kishony, R., Kahne, D. & Ruiz, N. Regulation of cell size in response to nutrient availability by fatty acid biosynthesis in *Escherichia coli*. *Proc. Natl. Acad. Sci. U.S.A.* **109,** E2561–2568 (2012).
37. Levin, P. A. & Angert, E. R. Small but Mighty: Cell Size and Bacteria. *Cold Spring Harb. Perspect. Biol.* **7,** a019216 (2015).
38. Wechsler, J. A. & Gross, J. D. *Escherichia coli* mutants temperature-sensitive for DNA synthesis. *Mol. Gen. Genet.* **113,** 273–284 (1971).
39. Gullbrand, B. & Nordstrom, K. FtsZ ring formation without subsequent cell division after replication runout in *Escherichia coli*. *Mol. Microbiol.* **36,** 1349–1359 (2000).
40. Løbner-Olesen, A., Skarstad, K. & HANSEN, F. G. The DnaA protein determines the initiation mass of *Escherichia coli* K-12. *Cell* **57,** 881–889 (1989).
41. Skarstad, K. & Katayama, T. Regulating DNA replication in bacteria. *Cold Spring Harb. Perspect. Biol.* **5,** 1–17 (2013).
42. Boye, E., Stokke, T., Kleckner, N. & Skarstad, K. Coordinating DNA replication initiation with cell growth: Differential roles for DnaA and SeqA proteins. *Proc. Natl. Acad. Sci. U.S.A.* **93,** 12206–12211 (1996).
43. Lu, M., Campbell, J. L., Boye, E. & Kleckner, N. SeqA: a negative modulator of replication initiation in *E. coli*. *Cell* **77,** 413–426 (1994).
44. Torheim, N. K., Boye, E., Løbner-Olesen, A., Stokke, T. & Skarstad, K. The *Escherichia coli* SeqA

474 protein destabilizes mutant DnaA204 protein. *Mol. Microbiol.* **37,** 629–638 (2000).
475 45. Wachi, M. *et al.* Mutant isolation and molecular cloning of mre genes, which determine cell shape,
476 sensitivity to mecillinam, and amount of penicillin-binding proteins in *Escherichia coli*. *J. Bacteriol.*
477 **169,** 4935–4940 (1987).
478 46. Levin, P. A., Margolis, P. S., Setlow, P., Losick, R. & Sun, D. Identification of Bacillus subtilis
479 genes for septum placement and shape determination. *J. Bacteriol.* **174,** 6717–6728 (1992).
480 47. Peters, J. M. *et al.* A Comprehensive, CRISPR-based Functional Analysis of Essential Genes in
481 Bacteria. *Cell* **165,** 1493–1506 (2016).
482 48. Hartwell, L. H., Hopfield, J. J., Leibler, S. & Murray, A. W. From molecular to modular cell biology.
483 *Nature* **402,** C47–52 (1999).
484 49. Brown, S. D. & Jun, S. Complete Genome Sequence of *Escherichia coli* NCM3722. *Genome*
485 *Announc.* **3,** e00879–15 (2015).
486 50. Neidhardt, F. C., Bloch, P. L. & D. F. Smith. Culture medium for enterobacteria. *J. Bacteriol.* **119**,
487 736-747 (1974).
488 51. Odsbu, I., Morigen & Skarstad, K. A reduction in ribonucleotide reductase activity slows down the
489 chromosome replication fork but does not change its localization. *PLoS ONE* **4,** e7617 (2009).
490 52. Youngren, B., Nielsen, H. J., Jun, S. & Austin, S. The multifork *Escherichia coli* chromosome is a
491 self-duplicating and self-segregating thermodynamic ring polymer. *Genes Dev.* **28,** 71–84 (2014).
492

Methods

No statistical methods were used to predetermine sample size.

Strain and oligo information

All experiments in normal growth conditions or with physiological perturbations were carried out using a prototrophic strain NCM3722 (*49*) unless otherwise noted. Specifically, a non-motile, F- derivative SJ358 was used. Thymine limitation and tCRISPRi experiments were based on strains with a MG1655 background (unpublished data). Detailed information of strain genotypes is included in Extended Data Table 1. Oligo information for strain construction and qPCR primers is in Extended Data Table 2.

Media and growth conditions

The growth medium for normal growth conditions, physiological perturbations by antibiotics or tCRISPRi is based on MOPS (*50*). The growth medium for thymine limitation is based on M9. The details of the media used are listed in Extended Data Table 3. Before every turbidostat experiment, cells were inoculated into 1 ml lysogeny broth (LB) medium as seed culture from a single colony on agar plate, streaked no more than 7 days before use. After 6-12 hours in 30°C or 37°C water bath shaker, cells were diluted 1000-fold into 1ml-2ml of the specific growth medium as pre-culture and shaken at 37°C in water bath until OD_{600} = 0.2. The pre-culture was then back-diluted 1000-fold again into the same medium and shaken at 37°C in water bath until OD_{600} = 0.2. The back-diluted culture was then inoculated into each turbidostat vial with or without specific inhibiting conditions, and the turbidostat experiment was started when $OD_{600} \approx 0.05$ for each vial. Turbidostat was then run for at least 8 generations in steady-state growth before sample collection. Samples that didn't show steady-state growth were discarded. In each turbidostat experiment, we were able to run up to 8 different growth conditions simultaneously. For each condition, samples were collected for cell size, RNA/protein and cell cycle measurements. The typical range of concentrations of antibiotics or inducer in gene knockdown we used is detailed in Supplementary Table 1.

Design of multiplex turbidostat (or TSTAT)

Different from the typical turbidostat which maintains a constant turbidity of the cell culture, our TSTATs are set to allow the accumulation of turbidity up to a preset threshold. Upon reaching this upper turbidity threshold each TSTAT dilutes its culture until a defined lower turbidity threshold. After dilution, the culture in each TSTAT grows continuously until the upper turbidity threshold is reached again. This process repeats and the culture maintains steady-state growth. The turbidity of the culture is measured at 15-second intervals. The individual exponential curves between consecutive dilutions can be fit to an exponential for measurement of the doubling times.

Each TSTAT has its own fixed-wavelength spectrophotometer for taking real time turbidity measurements. The spectrophotometer componentry of each TSTAT is built into a culture vial cup holder with one 600nm T-$1^3/_4$ form factor LED fitted into one end facing opposite to a 570nm (FWHM ~350nm) broad band T-$1^3/_4$ form factor phototransistor press fitted into the other end. With a culture vial

placed in the vertical bore of the holder, the LED and phototransistor act as a simple fixed-wavelength spectrophotometer. The LEDs are powered by a microcontroller board (Arduino Mega 2560) for each TSTAT and measurements of the current through the LEDs and the phototransistors of each TSTAT is done by taking voltage measurements across shunts in series. A Java GUI on a computer connected to the microcontroller board provides the main control and logging functionality including the ability to measure and set a blank value for each spectrophotometer.

Separate pneumatically driven media bottles supply each TSTAT with growth media for dilution. The flow in the dilution/media lines is mechanically controlled by pinch valves (Bio-Chem Fluidics, Inc., NJ). A regulated diaphragm pump supplies driving pressure (15kPa) to each media bottle as well as the compressed air flow which bubbles the cultures in each TSTAT vial to assure the aeration of the cell culture. A small stir bar provides additional agitation to the culture (Fig. 1a). All TSTAT experiments were performed at 37°C in an environmental warm room to avoid temperature fluctuation.

Growth rate measurement

The phototransistor current is read off an analog-digital converter (ADC) connected to the phototransistor shunt. Phototransistor current readings are measured at different light intensities and an intensity-current (each normalized relative to its respective maximum value) curve was fit to a second-order polynomial. Cell cultures measured at different OD_{600}s were fixed and the working curve of a normalized intensity and OD_{600} was mapped out and used to convert the readings from phototransistor currents to actual OD_{600}. $OD_{600}=-(1/\alpha)\times\ln(I_{norm}/I_{black})$, where α is the slope of the normalized intensity-OD_{600} curve.

The OD_{600} vs. time curve was fit to a single exponential $I = I_0\, 2^{t/\tau}$ for each segment between two consecutive dilution events and the average was taken as the generation time. Growth rate is given by $\lambda = \ln 2/\tau$. Each turbidostat was blanked with the media used in experiment.

To ensure exponential growth, cells were kept between $OD_{600} = 0.05$ and $OD_{600} = 0.20$. Once the OD_{600} reaches 0.20, the vial was diluted automatically until $OD_{600} = 0.05$ (Fig 1a). The OD vs. time curve was fit to a single exponential $I = I_0\, 2^{t/\tau}$ for each segment between two consecutive dilution events and the average was taken as the generation time. Growth rate is given by $\lambda=\ln 2/\tau$. Each turbidostat is blanked with the same media before each experiment.

Sample collection from TSTAT and preparation for imaging

Cell samples were collected when cell culture reached $OD_{600} = 0.2$ or 0.4 (*18*). Typically 20ml of cell culture would be collected and kept on ice immediately to prevent further growth or dramatic change of cell physiology. From the same culture, cell samples were collected for cell size, genomic DNA for qPCR, image cytometry, RNA/protein and transcription level (typically together with cell size measurements), respectively.

Before imaging, cells were concentrated to an appropriate cell density by centrifuging and removal of excess supernatant. 0.1mM 2-mercaptoethanol (Sigma) was added to reduce cell clumping. Cells were pipetted onto an agarose pad made by 0.2% w/v agarose (Genesee Scientific, CA). The agarose pad was then flipped and put onto a Willco dish (WillCo Wells B.V.) with a glass coverslip on top to reduce the evaporation during imaging.

Microscopy and image acquisition

All transmission light and fluorescence microscopy were performed on an inverted microscope (Nikon Ti-E) with Perfect Focus 2 (PFS 2), 100x oil immersion objective (PH3, NA=1.45), LED fluorescent light (Lumencor Inc., OR), and Andor NEO sCMOS camera (Andor Technology Ltd., MA). Exposure time was between 100-200ms with 100% transmission. From each set of sample, 140-300 images were captured and 5,000-30,000 cells were analyzed to ensure statistically significant distributions of cell measurements such as cell size or DNA content. All cell image analysis was carried out by custom software written in Python-OpenCV. Code can be provided per request to the authors.

Cell size measurement

Cell samples were fixed with 0.24% w/v formaldehyde in the same growth media and imaged within 24 hours. Image analysis extracted the contours of all possible items from phase contrast images, and these were primarily filtered based on shape and size. The probability distribution of contour width is symmetrical and not correlated width cell length (*12*). All filtered contours within 3 standard deviations from the mean value of the distributions were kept and exported as isolated images for re-examination. Cell size as well as surface area were calculated as a cylinder with two hemispherical ends for rod-shaped cells. The aspect ratio was calculated as the ratio of length to width of cell contour. We also validated the cell size measurement by using a total cellular protein staining measurement and applied it to irregular cell shape in thymine limitation and MreB knockdown (see Supplementary Information) (*51*).

The precision of cell size measurement by phase contrast image was also confirmed by total cellular protein staining measurement as described previously (*51*). Standard cells with known cell size were stained with a secondary dye WGA (wheat germ agglutinin conjugated with texas red binds to cell wall, similar to that used in the DNA content measurement below) and then mixed with experimental cells. The mixture of cells was then washed with 0.1M KH_2PO_4/K_2HPO_4 at pH 9.0 and resuspended in phosphate buffer (PB). Next, cells were stained with 3μg/ml of freshly made fluorescein isothiocyanate (FITC) at 4°C overnight. Before imaging, cells were washed and resuspended in TBS buffer (20mM Tris-HCl pH 7.5, 130mM NaCl). The image analysis shows that the ratio of cell size based on cell contour or protein staining measurements is consistent between standard and experimental cells.

RNA/protein measurements

Total protein quantitation. Total protein was measured as previously reported (*18*) except for the following modifications for sample collection. For some nutrient conditions, cells were collected when OD_{600}=0.2, so 6 ml cell culture was collected.

Total RNA quantitation. Total RNA was measured as previously reported (*18*) except for the following modifications for sample collection. For some nutrient conditions, cells were collected when OD_{600}=0.2, so 6 ml cell culture was collected. The cells were pelleted by centrifugation, washed once with 1 ml water, centrifuged again and the pellet fast frozen on dry ice.

C period measurement by qPCR

Genomic DNA was prepared using phenol-chloroform extraction. Cell samples from TSTAT were fast-frozen on dry ice for storage if not treated immediately. Frozen samples were thawed, pelleted and resuspended with TES buffer (10mM Tris pH 8, 1mM EDTA pH 8, 0.6% w/v SDS, 0.12mg/mL proteinase K, 250µl per 1 ml of culture). Samples were incubated at 65°C for 15 minutes, after which equal volume of phenol:chloroform (1:1) was added and mixed by vigorous vortexing. Each sample was centrifuged for 5-10 minutes to facilitate phase separation and the aqueous phase was transferred to a new tube before extracting again using 30% volume of chloroform. The aqueous phase after the second cleaning was again transferred to a new tube and sequentially mixed with 10% volume of 3M sodium acetate (pH 5.2) and 30% isopropanol. All samples were centrifuged at 4°C for 15 minutes to allow for precipitation of DNA. The supernatant was decanted and tubes air dried at room temperature. DNA samples were dissolved in Tris buffer (pH 8.0) and quantified using a Nanodrop 2000 (Thermo Scientific).

Each qPCR reaction was carried out with PowerUp SYBR Green Master Mix (ABI) with 10 ng of DNA template in a 20µl reaction using a Mx3000P qPCR system (Agilent Technologies). All primers were designed such that the size of each amplicon/genomic locus is about 100bp with similar annealing temperatures. The specificity of PCR amplification was validated by inspecting the melting curves of each reaction. Fluorescence time traces from the qPCR system typically have a sigmoid shape (Extended Data Fig. 1a). All traces were background-subtracted and fit to a single exponential at the amplification stage, from which the amplification efficiency (the exponential, $\alpha \in (1,2]$) was derived. The threshold value (H) was determined as the interpolated replication cycle number (down to two digits) at which the fluorescence signal rises above a given threshold within the exponential phase. The exact value can be varied without affecting the final results. DNA amplification can be simplified as an exponential increase such that $[DNA]_c = [DNA]_0 \times \alpha^H$ with $\alpha = 2$ in an ideal PCR reaction. Therefore, the amount of initial DNA is exponentially dependent on H and $-(H_1-H_2)$ reflects the relative abundance of two genomic loci in the sample. As discussed below, the ratio of DNA abundance from two genomic loci is also exponentially dependent on the ratio of C/τ.

Here we briefly show how we can use $-\Delta H$ to derive C period. Given an exponentially growing population of cells, the average copy number of a chromosomal locus X is a function of its distance g

from the *oriC*: $\langle X \rangle = 2^{(1-g)C+D/\tau}$, where $g \in [0,1]$, $g = 0$ for *oriC* and $g = 1$ for *ter*. The ratio of copy numbers from two loci is thus determined by $\langle X_1 \rangle / \langle X_2 \rangle = \alpha^{-(H_1-H_2),}$ the logarithm of which gives the ratio C/τ. Therefore, we have $C/\tau = \log_2\alpha \times (\Delta H/\Delta g)$. We checked the linearity of ΔH over Δg for foci falling onto the left or right arm of the chromosome respectively, and they behaved as expected (Extended Data Fig. 1b). Given the doubling time from TSTAT experiments, C periods can thus be calculated. Detailed derivation of the above equations is discussed in Supplementary Information. All combinations of foci pairs from the same chromosome arms were calculated and the median was taken as the replication period estimate. A total of 8 pairs of primers were selected, 3 pairs targeting the *oriC*, 3 pairs targeting the *ter* and 2 pairs targeting the middle of the left and right arms respectively. We also compared this estimate from a more comprehensive dataset based on 26 pairs of primers evenly distributed along the chromosome, the results agreed with each other (Extended Data Fig. 1b).

DNA content measurement

Instead of flow cytometry, we used an imaging method to acquire both DNA content and cell morphological information. To precisely measure the DNA content in each cell, standard cells with known copy number of DNA were used. Wild type NCM3722 or MG1655 cells cultured in slow growth condition MOPS + 0.2% mannose with typical doubling time around 90 minutes were treated with 150μg/ml rifampicin and 10μg/ml cephalexin for 6-6.5 hours (also known as a run-out experiment). The run-out cells contain one or two copies of DNA (Extended Data Fig. 1e).

Both experimental cells from TSTAT culture and standard cells were washed with TE buffer (10mM Tris-HCl, pH 7.5, 1mM EDTA) and fixed with 70% ethanol for at least 12 hours at 4°C. Before imaging, the standard cells were washed by TBS and stained with 80μg/ml wheat germ agglutinin conjugated with Oregon Green 488 or Alexa Fluor 594 (WGA 488 or 594) for 1-1.5 hours. Then the standard cells were washed with TBS twice and mixed with experimental cells. All cells were then stained with 3μg/ml Hoechst 33342 dye for 45 minutes on ice.

Phase contrast and two-color fluorescent images were then captured for an order of 10^4 cells. Experimental and standard cells were separated by gating out the WGA signals (Extended Data Fig. 1d). The probability distributions of DNA content of two populations of cells were then plotted together. The mean position of the high peak in standard cell indicating two copies of DNA was used to calibrate the average DNA content of experimental cells (Extended Data Fig. 1e).

Run-out experiments were also performed to calculate cell cycle parameters. Similar to exponentially growing cells, experimental cells in different media were run out by treating with 150μg/ml rifampicin and 10μg/ml cephalexin for 6-6.5 hours, and then washed and fixed in ethanol as described above. Again, staining and imaging were done together with standard cells. The calculations of DNA copy number using the two methods are consistent (see Supplementary Information).

Foci detection at *ori*

Cell strains with ParS-ParB labeling different chromosome loci were used to count the number of replication origins directly (See Extended Data Table 1). Cells were cultured in TSTAT and then collected for foci imaging and cell size and cell cycle measurements. It was shown that in MOPS + 0.2% mannose with typical doubling time around 90 minutes where cells presumably have one or two overlapping cell cycles, the number of different foci (84.3' and 54') was consistent with the theoretical prediction (Extended Data Fig. 3d; Supplementary Information), and the cell size per *ori* calculated from different foci was also consistent. However, in faster growth conditions such as MOPS + 0.2% glucose with typical doubling time around 40 minutes where cells have 2-3 overlapping cell cycles, the number of overlapping cycles as well as copy number of DNA increased. This caused an underestimation of foci number (Extended Data Fig. 3g). It is likely because of the cohesion of chromosomal foci beyond the diffraction limit that we could not detect all foci here.

Estimation of gene transcription level in tCRISPRi strains

The transcription level of the knocked down gene was estimated by a co-transcribed fluorescence reporter mfsGFP. Although protein expression may vary between the co-transcribed genes because of their different translation efficiencies[15], their relative expression level can be estimated by the transcriptional activity, which is correlated to the translation level at the population level. The cells of tCRISPRi strains were fixed with 0.24% w/v formaldehyde and imaged within 24 hours of fixation. Both phase contrast and fluorescent images were obtained. Background subtraction was done by fitting a gaussian to the spectrum of background intensities and subtracting the peak value from each cell. The expression level of fluorescence reporter per cell was estimated as the total fluorescence intensity per cell volume. Therefore the percentage of reduction in average total fluorescence per cell as compared to the uninduced group was used as a proxy of transcription level of the gene under study.

Author Contributions

F.S, D.L., S.C., J.S., O.A., A.S., M.E., Y.J., X.L. conducted experiments. F.S, D.L., S.C., J.S., O.A, S.J. analyzed data. S.J. designed the research. F.S., D.L., S.C., and S.J. wrote the paper.

Acknowledgements

This work was supported by the Paul G. Allen Family Foundation, Pew Charitable Trust, NSF CAREER, and NIH R01 GM118565-01 (to S.J.). We are deeply grateful to Terry Hwa, Petra Levin, Kirsten Skarstad, Massimo Vergassola, and all members of Jun lab for invaluable discussions. Special thanks to Tony Hui for help with RNA/protein measurements in the initial stage of this work.